Ocean Engineering 266 (2022) 112658

Contents lists available at ScienceDirect

Ocean Engineering

journal homepage: www.elsevier.com/locate/oceaneng

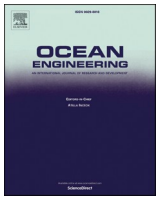

Numerical investigation into the effects of tip vortex cavitation on propeller underwater radiated noise (URN) using a hybrid CFD method

Savas Sezen [a,b,*], Mehmet Atlar [b]

[a] Lloyd's Register (LR), EMEA, UK
[b] Department of Naval Architecture Ocean & Marine Engineering, University of Strathclyde, Glasgow, UK

ARTICLE INFO

Keywords:
AMR
Cavitation
CFD
DES
FWH
URN
The Princess Royal
TVC

ABSTRACT

This study explores the influence of tip vortex cavitation (TVC) on propeller induced URN using a hybrid CFD method. The cavitating flow around the model and full-scale benchmark propeller belong to the Newcastle University's research vessel, The Princess Royal, operating under uniform, inclined and non-uniform flow conditions were solved using DES and mass transfer model. The recently developed advanced mesh refinement (V-AMR) technique was incorporated into the calculations for better modelling tip vortex flow and realising the TVC in the propeller slipstream. This technique enabled the inclusion of the nonlinear noise sources, mainly represented by turbulence and vorticity, including TVC, effectively for the accurate prediction of propeller URN. The numerical calculations were conducted in conditions where only the sheet cavitation was modelled without the V-AMR technique and where the sheet and tip vortex cavitation was modelled together using the V-AMR technique to understand the contribution of TVC to the overall propeller URN. The results were first validated with the available experimental data obtained in the model scale test campaign in the cavitation tunnel and sea-trial data for the propeller's hydrodynamic performance characteristics, cavitation extensions and URN. The results showed that the contribution of TVC to the overall propeller URN was minimal in conditions where the stable and structured TVC was present (i.e., under uniform flow conditions). However, when the propeller was operating under inclined and non-uniform flow conditions where the cavitation dynamics and vortex pulsation were dominant, the unstructured and unstable TVC was observed compared to the observations of TVC under uniform flow conditions. The unstructured TVC created several spikes, which can be associated with its strong cavitation dynamics and possible collapsing/bursting phenomena. These spikes created by the TVC and observed in the time domain acoustic pressure signal consequently contributed to the propeller URN at the different frequency ranges of the noise spectrum and increased the URN levels up to 15 dB under non-uniform flow conditions compared to the propeller URN predictions when only the sheet cavitation was present.

1. Introduction

Almost all ship propellers are operating under cavitating conditions to reach optimum performance, and hence its avoidance is almost inevitable. Amongst the several side effects of cavitation, in particular, cavitating propeller noise is one of the major noise sources for ships. It needs to be reduced not only to increase passengers' and crews' comfort but also to decrease the possible short and long term negative impacts on marine fauna (van Terwisga, 2006; Wijngaarden, 2011; Bosschers, 2018).

Depending on the operating conditions, various cavitation forms (e.g., sheet, bubble, cloud, vortex cavitation) can be observed on the ship propellers, and their effects on the hydrodynamic and hydroacoustic performance of a propeller are different. The most commonly observable cavitation types on the ship propellers and most relevant for underwater radiated noise (URN) are the sheet and tip vortex cavitation (TVC). Although sheet cavitation is considered more harmful than vortex cavitation, TVC is the first type of cavitation that occurs on well-designed propellers. Hence, accurate modelling and prediction of its noise are of critical importance. This is because the TVC is deemed the main cavitation type controlled in the propeller design stage (Asnaghi et al., 2020b). It is generally associated with broadband hull-pressure fluctuations, broadband noise, and rudder erosion in many cases (Bosschers, 2018).

* Corresponding author. Lloyd's Register (LR), EMEA, UK.
E-mail address: savas.sezen@lr.org (S. Sezen).

https://doi.org/10.1016/j.oceaneng.2022.112658
Received 18 May 2022; Received in revised form 1 September 2022; Accepted 17 September 2022
Available online 8 October 2022

Several numerical methods (e.g., potential and viscous based solvers) have been used for cavitation modelling. However, within the limitations of the current numerical models, sheet cavitation is the only form of cavitation that is modelled (e.g., Taehyung et al., 2016; Bensow and Liefvendahl, 2016). The reason is that the vortex core has anisotropic turbulence and high-velocity gradients in three directions, which makes the accurate prediction of minimum pressure inside the tip vortex and TVC difficult (Asnaghi et al., 2020a). Due to this fact, the solution of the tip vortex and hence TVC require advanced numerical methods and grid structures compared to sheet cavitation modelling. In order to overcome this issue, the priory local mesh refinements (i.e., tube and spiral) are generally applied at the blade tips to adopt sufficient cells inside the vortex core to model the TVC in the propeller slipstream. However, these applications are not successful compared to applying the local grid refinements along the tip vortex trajectory using the newly adopted Adaptive Mesh Refinement (AMR) techniques. In this regard, different AMR procedures have been developed and used for better modelling the TVC in the propeller slipstream (e.g., Lloyd et al., 2017; Krasilnikov, 2019; Sezen and Atlar, 2021; Kimmerl et al., 2021).

In order to gain further information on the mechanism of TVC, cavitating propeller URN has become an important research field. However, most authors have focused on cavitation on the propeller so far as the influence of developed TVC on broadband and narrowband noise is not yet fully understood both numerically and experimentally (Higuchi et al., 1989; Strasberg, 1986). In the past, only a few experimental studies were conducted to address the TVC noise for marine propellers and foils specifically. As stated in Pennings et al. (2016), Barker (1976) studied the source of cavitation noise experimentally and found out that the steady tip vortex cavity did not show the strong collapse of other types of cavitation and thus produced less sound. The findings were also observed in other studies solely focusing on steady cavitating trailing tip vortices (e.g., Higuchi et al., 1989; Maines and Arndt, 1997; Astolfi et al., 1998). Konno et al. (2002) conducted a comprehensive experimental study to investigate the bursting or collapsing phenomenon of TVC by changing the wake distributions, thrust coefficients and cavitation numbers using two different marine propellers. The pressure fluctuations were measured to understand the effects of systematic investigations. The results showed that large pressure hull fluctuations occurred twice in the bursting phenomenon, and they strongly depended on the wake distribution. Also, it was found that the stabilisation of TVC or total cavitation volume reduction needed to be achieved to suppress the TVC. Pennings et al. (2016) explored whether the resonance tip vortex cavity was the main source of high-amplitude broadband pressure fluctuations for a full scale propeller by conducting a series of experiments in the cavitation tunnel. Additionally, the Proctor vortex model was used to determine the resonance frequency of the tip vortex cavity. The experimental measurements showed that steady tip vortex cavitation in the propeller slipstream did not yield a significant sound in uniform flow in the range of 0.5–1.2 kHz. In contrast, the noise levels increased in the presence of the upstream wake. It was found out that dominant sound frequency was directly associated with the resonance of the tip vortex cavity.

Similar to experimental studies, various semi-empirical formulations have also been utilised to predict TVC noise in the literature. Raestad (1996) developed a semi-empirical formulation called Tip Vortex Index (TVI) based on the pressure field generated by the cavity volumes on the propeller blades using the measurements conducted for Queen Elizabeth 2. The results obtained by the semi-empirical formulation were found in line with the measurements. Lafeber et al. (2015) studied the cavitating propeller URN for the container, cruise and catamaran vessels using different computational models (i.e., propeller flow panel method (PROCAL), tip vortex noise model (ETV), sheet cavitation noise model (Matusiak and Brown)). The numerical results were compared with the full-scale sea trials and measurements conducted in the depressurised water tunnel in MARIN. The results showed that the ETV model predicted the noise in good agreement with the sea-trial data for the cruise liner as the vortex cavitation was expected to be dominant. However, ETV underpredicted the noise levels for a container vessel compared to experimental data measured in the cavitation tunnel as there was significant sheet cavitation observed on the blades. In a recent comprehensive study, Bosschers (2018) developed prediction methods for broadband noise, including hull pressure fluctuations generated by the developed tip vortex cavitation using the full-scale and model scale data. In his model, the vortex cavity size was the principal parameter, and it was predicted with the boundary element method and together with the semi-empirical vortex model. Also, the conducted several computations and formulations were also utilised to develop a novel method for model tests to correct the scale effects due to the Reynolds number on broadband noise of TVC. The developed model could predict the broadband hull-pressure fluctuations and URN using the inputs provided by the boundary element method (BEM) and acceptable results were obtained compared to experimental and sea trial data for different propellers and operating conditions. Berger, 2018 carried out comprehensive investigation for the interaction of sheet and tip vortex cavitation and higher-order hull pressure fluctuations. In the author's dissertation, it was found out that the interaction between the sheet and tip vortex cavitation was main driving mechanism for the high-order pressure fluctuations. Another comprehensive investigation on vortex characteristics were performed by Feder (2021). In his dissertation, the hybrid RANS-LES model was used to examine the vortex flow and its characteristics. Several important findings were presented for the vortex flows Sezen and Bal (2020) investigated the TVC noise at the inception stage using the potential based semi-empirical TVI (Tip Vortex Index), developed by Raestad (1996) and hybrid viscous methods in open water conditions. The numerical results showed that the TVI and hybrid method gave the same results once the TVC started. Thus, it was stated that the TVI method could be reliably applied instead of the hybrid method at the inception stage of TVC.

In recent years, with the development of computational tools, cavitating propeller URN has been predicted using the hybrid CFD method, which is the combination of hydrodynamic solver and acoustic analogy. The flow field is decoupled in this method, and noise sources and sound radiation are computed separately. The sound radiation part can be considered a post-processing step based on the application of acoustic analogies. Amongst the different acoustic analogies, the most commonly used one is the Ffowcs Williams Hawkings (FWH) (Ffowcs Williams and Hawkings, 1969) equation for both aeroacoustics and hydroacoustic applications. In particular, applying a permeable formulation of the FWH equation is a new approach to effectively solving nonlinear noise sources' contributions in the hydroacoustic field. Although there is no general consensus related to the application of permeable formulation of the FWH equation in the literature, there are several papers that utilised the permeable FWH formulation and showed its effectiveness to explore the contribution of nonlinear noise sources under non-cavitating and cavitating conditions (e.g., Ianniello et al., 2013; Ianniello et al., 2014a; Ianniello et al., 2014b; Testa et al., 2018; Lidtke et al., 2019; Sezen et al., 2020; Testa et al., 2021). However, the cavitating propeller URN is generally predicted by modelling only the sheet cavitation on the propeller blades due to the modelling difficulties of cavitating tip vortices stated before (e.g., Lidtke et al., 2016; Stark and Shi, 2021). Also, the lack of reproduction of cavitating tip vortices in the numerical calculations is considered to be the main reason for the underprediction of propeller URN levels in the numerical calculations compared to experimental data (e.g., Bensow and Liefvendahl, 2016; Fujiyama and Nakashima, 2017; Li et al., 2018).

Within the above context, in our recent study (Sezen and Atlar, 2021), we developed and presented the Vorticity-based Adaptive Mesh Refinement (V-AMR) technique for better representation of TVC in the propeller slipstream. In this recent study, the capabilities of the different numerical methods (e.g., RANS, DES and LES) and effects of numerical modelling parameters (e.g., grid and time step resolution) were comprehensively investigated. The proposed method enabled TVC

modelling with a minimum computational cost. The present study has extended the recent investigation further by exploring the effects of TVC on propeller hydroacoustic performance using the developed V-AMR technique for the existing benchmark research vessel propeller, The Princess Royal. As the TVC is the first type of cavitation observed on well-designed propellers, its noise and contribution to the overall propeller URN are of great interest. Also, to the best of the authors' knowledge, the contribution of TVC to the overall propeller hydroacoustic performance has not been explored yet for model and full-scale propellers using CFD. Thus, this study aims to understand the contribution of TVC on the overall propeller URN levels at different operating conditions for model and full-scale benchmark propellers.

In this study, the cavitating flow around the model and full-scale benchmark propeller operating under uniform, inclined and non-uniform flow conditions was solved using the DES method and Schnerr-Sauer cavitation model. The developed V-AMR technique was applied for a better representation of TVC in the propeller slipstream. In order to understand the contribution of TVC to the overall propeller URN, the numerical calculations were carried out in conditions where only sheet cavitation was modelled as well as the sheet and tip vortex cavitation in combination by using the V-AMR technique for modelling the latter. The numerical results were first validated with the available experimental data obtained in the model scale test campaign and full-scale measurements for the propeller hydrodynamic performance characteristics, cavitation extensions and URN. Following this, a detailed investigation to understand the effects of TVC on propeller URN was conducted in the time and frequency domain at different operating conditions.

The structure of the paper is organised as follows. Section 2 presents the theoretical background, including hydrodynamic and hydroacoustic models, whereas Section 3 presents the numerical modelling, including the computational domain, grid structure, and analysis properties. The hydrodynamic results, cavitation extensions and URN predictions are presented in Section 4. Finally, the concluding remarks are given in Section 5.

2. Theoretical background

2.1. Hydrodynamic model

Cavitation is an important flow phenomenon that can occur in many flows. Most engineering flows in which the cavitation occurs are turbulent. Thus, the flow around the ship and propeller is an excellent example of a full-scale turbulent flow. Cavitation causes several detrimental effects on marine propellers, and they can be mainly classified as follows.

- Performance loss
- Noise
- Vibration
- Erosion

In order to reduce the harmful effects of cavitation on propeller hydrodynamic and hydroacoustic performance, it is, therefore, crucial to predict the cavitating flow accurately to apply mitigating measures. In this regard, CFD tools play an important role in predicting cavitation flow around the marine propellers both in model and full-scale. In general, mass transfer cavitation models are utilised in the CFD solvers. Within the facilities of a commercial CFD solver, Star CCM+ 14.06 (Star CCM+ 14.06, 2019), used in this study, the cavitation modelling is based on the homogenous two-phase flow assumptions. The motion equations are solved for a single effective fluid, and an additional equation enables the determination of vapor and liquid phase for the vapor volume fraction. Under the homogenous two-phase flow assumptions, seeds are spherical, uniformly distributed in the liquid, and initially have the same radius. To determine the bubble growth rate, the Schnerr Sauer cavitation model, based on the reduced Rayleigh-Plesset equation, was used in this study by neglecting the inertial term, surface effects and viscous diffusion (Schnerr and Sauer, 2001; Muzaferija et al., 2017; Star CCM+ 14.06, 2019). In addition to the cavity dynamics, the interaction between turbulence and cavitation is critical for accurately representing cavitation. For instance, standard RANS methods overpredict the turbulent viscosity around the cavity region, which resulted in an insufficient extension of vortex cavitation (i.e., hub or tip vortex cavitation) in the propeller slipstream. Also, due to the anisotropic turbulence and high gradients inside the vortex core, the standard RANS methods are not capable to capture these details compared to advanced numerical methods (i.e.,DES and LES). Although standard RANS methods are generally applied at the preliminary design stage to obtain the overall idea about the cavitation, they are also not successful in capturing the unsteady behaviour of cavitation compared to scale resolving simulations. Therefore, scale resolving simulations (i.e., DES and LES) are the alternative ways to model the cavitation and turbulence to provide accurate interaction.

This study utilised the DES method to combine the RANS in the boundary layer and LES in the propeller slipstream. Thus, this method is a good compromise for accurately capturing the flow details that RANS is not capable of and without the high computational effort required by LES, particularly through near-wall modelling. Amongst the different variants of the DES method, DDES (Delayed Detached Eddy), the upgraded version of the standard DES method, was used with the k-ω SST turbulence model. DDES method incorporates a delay factor that improves the model's ability to separate between LES and RANS regions. In this way, the RANS and LES regions inside the computational domain can be distinguished (Star CCM+ 14.06, 2019 and Spalart et al., 1997). In our case, the RANS method provided the boundary layer solution, whereas LES was used to resolve flow details in the propeller slipstream for model and full-scale applications. The formulations are not repeated here, and they can be found in the user guide of the CFD solver (Star CCM+ 14.06, 2019).

2.2. Hydroacoustic model

The DDES method was used to assess flow field solution in the near field, and hence the required inputs for the acoustic analogy were provided by the DDES method for the sound propagation. In this study, FWH (Ffowcs Williams and Hawkings, 1969) acoustic analogy was used for the noise propagation from near to far-field. This acoustic analogy is derived by rearranging the governing equations (i.e., continuity and momentum) into the nonhomogeneous wave equation with source terms. Amongst the different integral based acoustic analogies, a permeable formulation of the FWH equation was used in this study to include the contribution of nonlinear noise sources, mainly represented by turbulence and vorticity, including TVC, effectively. The influence of cavitation on the blades will be more dominant on overall propeller URN than the contribution of nonlinear noise sources when the propeller operates under cavitating conditions. However, the turbulent and vorticity structures resolved by the DES method and TVC also contribute to the overall noise level. Hence, nonlinear noise sources need to be taken into account for the accurate prediction of propeller URN.

The permeable FWH formulation, first implemented and proposed by Ffowcs Williams and Hawkings (1969) and proposed as a possible numerical solution of the FWH equation by Di Francescantonio (1997), requires a fictitious integral surface. This integral surface encompasses the propeller and the relevant portion of the propeller slipstream to account for the contribution of nonlinear noise sources, including TVC. The permeable FWH formulation can be derived by introducing modified velocity (U) and stress tensor (L) using the generalised formulation of the FWH equation, and it can be written as follows (Farassat, 2007);

$$\Box^2 p = \frac{\partial}{\partial t}\left[\rho_0 U_n\right]\delta(f) - \frac{\partial}{\partial x_i}\left[L_i\delta(f)\right] + \frac{\partial^2}{\partial x_i \partial x_j}\left[T_{ij}H(f)\right] \quad (1)$$

Here, $\square$ is the wave or D'Alembertian operator in three-dimensional space, n is unit outward normal, ρ_0 is the speed of density in the undisturbed medium, p is the acoustic pressure, T_{ij} is the Lighthill stress tensor. $\delta(f)$ and $H(f)$ are the Dirac delta and Heaviside functions, respectively. In this equation, the first term represents the pseudo-thickness, while the second is the pseudo-loading noise term. The last term is the quadrupole (or nonlinear noise) term outside the integral surface. The permeable FWH formulation enables the evaluation of the nonlinear noise sources encapsulated by the integral surface using the surface integral. This makes the formulation very appealing because the solution of volume integral using the generalised FWH equation is computationally expensive and requires high computational memory. However, when the vortices pass through the downstream end of the permeable surface, they can create spurious noise due to truncation errors of the source terms at the integration boundary. Thus, this spurious noise can contaminate the acoustic prediction. This is also known as the end-cap problem in literature (Nitzkorski, 2015; Wang et al., 2018), and several special techniques are implemented, which are beyond the scope of our study. Alternatively, the complete FWH equation, including the volume integral terms outside the integral surface, can be solved to remove this issue completely (Testa et al., 2021). Yet, this will increase the computational cost of the solution considerably. In our study, the contribution of quadrupole noise sources outside the integral surface was neglected, and the end-cap problem was not investigated.

A small permeable surface encapsulating the propeller and part of its slipstream was used in this study based on our understanding of the flow field and verification studies conducted with different permeable surfaces, as there is no consensus about the permeable surface placement and dimensions in the literature. This permeable surface enables information loss mitigation, and it allows the include the most energetic part of the vortex structures emanating from the propeller blade tips in the propeller slipstream.

3. Test case set-up and numerical modelling

3.1. Propeller geometry and test matrix

The propeller used in this study belongs to a research vessel of Newcastle University, The Princess Royal (Atlar et al., 2013). This propeller has been recently recommended as a benchmark propeller because of the large amount of experimental and sea trial data through the cavitation observations and URN obtained by different European projects (e.g., SONIC, 2012) and ongoing round-robin (RR) test campaign (e.g., Tani et al., 2020). The main specifications of the propeller are given in Table 1, whereas Fig. 1 shows the 3D view of the propeller.

In order to explore the influence of TVC on propeller URN, the propeller was operating under uniform, inclined and non-uniform flow conditions both in model and full-scale. These conditions were determined according to the experiments conducted in different facilities in the round-robin (RR) test campaign and available sea trial data. For the non-uniform flow configurations, the propeller was operating in open water conditions and the wake field was used at the inlet of the computational domain. The wake field was measured in the Ata Nutku towing tank of Istanbul Technical University (ITU) using the Princess Royal vessel (Korkut and Takinaci, 2013). Thus, the complete hull, including appendages, was not modelled, resulting in simplifying the numerical solution and reduced computational cost. Fig. 2 shows the target wake field, obtained by towing tank and the simulated wake field used in the cavitation tunnel to replicate the same wake field as obtained in the towing tank. The simulated wake field was changed iteratively using a 2D wire mesh and LDV measurement device in the cavitation tunnel until the agreement between the target and simulated wake field was satisfied (Tani et al., 2019a).

Table 1
The main particulars of the propeller (Atlar et al., 2013).

Parameters	Model Scale	Full Scale
Diameter, D (m)	0.22	0.75
P/D at 0.7R	0.8475	0.8475
Expanded Blade Area Ratio (EAR)	1.057	1.057
Blade Number, Z	5	5
Rake (°)	0	0
Skew (°)	19	19

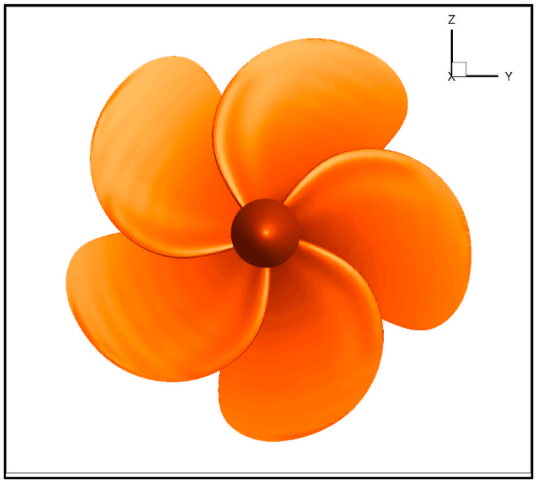

Fig. 1. 3D view of the benchmark Princess Royal propeller.

The operating conditions used in this study are summarised in Table 2. Here, J is advance ratio, β is the shaft or inclination angle, n is propeller rotational rate (rps), σ_N is the cavitation number, calculated based on the propeller rotational rate as follows.

$$\sigma_N = \frac{P_0 - P_V}{0.5\rho(nD)^2} \tag{2}$$

where, P_0 is the static pressure, P_V is the vapor pressure, and ρ is the water density.

Using the operating conditions given in Table 2, the propeller is operating in a condition where only sheet cavitation is present and also where the sheet and TVC are present together. In this way, the contribution of TVC to the overall propeller URN can be distinguished.

3.2. Numerical modelling

3.2.1. Computational domain and boundary conditions

The computational domain and its dimensions are created according to the University of GENOA cavitation tunnel (UNIGE) test section to replicate the same conditions in the numerical calculations for the model scale propeller. According to the test section, the total length of the domain was set to 2.2m with 0.57m height and 0.57m width. As shown in Fig. 3, the positive X direction is defined as velocity inlet, whereas the negative X direction is defined as pressure outlet. The remaining surfaces, including blades, hub, and shaft, are defined as walls with no-slip boundary conditions. The computational domain is divided into three different regions. A cylinder, which serves as a rotating region, is created around the propeller to define the propeller's rotational motion. Also, another big cylinder, which serves as a permeable surface, is placed around the propeller, and it encapsulates some part of the propeller slipstream. Another region is the static region, where the non-rotating part of the domain is embedded. The transitions between static and noise regions and between rotating and noise regions are provided with the internal interfaces. The constant velocity is assumed at the inlet of the computational domain under uniform and inclined flow conditions,

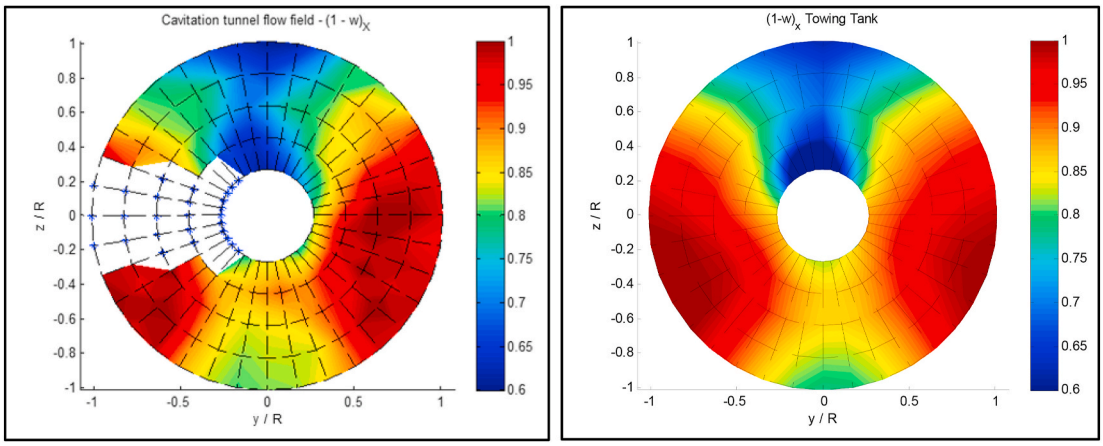

Fig. 2. Nominal wakefield at the propeller plane (Left: simulated wakefield in the cavitation tunnel, right: target wakefield measured in the towing tank) (Tani et al., 2019a).

Table 2
Operating conditions for model and full-scale propellers.

Uniform and Inclined Flow Conditions				
Condition ID	J	Shaft Angle (β,°)	n (rps)	σ_N (−)
C1	0.4	0	35	1.30
C2	0.4	5	35	1.30
C3	0.4	0	19.025	1.06
C4	0.5	0	19.025	1.06
Nonuniform Flow Conditions				
Condition ID	Engine RPM	STW (kn)	n (rps)	σ_N (−)
C5	2000	15.11	35	1.07
C6	2000	15.11	19.025	1.07

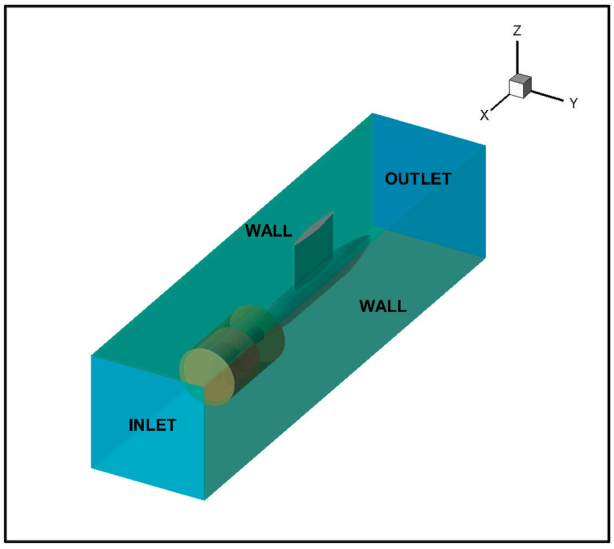

Fig. 3. Representation of computational domain used in the numerical calculations.

while the wake field is imposed at the inlet of the domain for non-uniform flow configurations. The computational domain was also created separately for the full-scale propeller. The domain was extended 4D towards the inlet and 16D towards the outlet from the blade centre. The radial distance was also set to 5D. Similar boundary conditions were used as in the model scale.

3.2.2. Grid generation

The grid quality is one of the crucial parameters in the numerical calculations affecting the solution's accuracy. Thus, the grid should be sufficient to solve the flow field around the propeller accurately. In particular, tip vortex flows are the most challenging flows because of the anisotropic turbulence and large gradients in three directions inside the vortex core (Asnaghi et al., 2020a). The accurate prediction of tip vortex flows is strongly dependent on grid resolution inside the vortex and turbulence modelling. The standard and traditional methods (e.g., local mesh refinements) are generally applied at the propeller blade tips to solve the tip vortex flow accurately and, hence, observe the tip vortex cavitation (TVC). Yet, they are not sufficiently successful and computationally expensive. When the full-scale propeller and non-uniform wake field is concerned, this becomes a more complex issue in the numerical calculations.

As known, TVC occurs on well-designed propellers as a first type of cavitation that contributes to the overall noise levels and can also cause rudder erosion. Therefore, the influence of TVC needs to be included in the numerical calculation. In this regard, the authors have recently introduced the Vorticity-based Adaptive Mesh Refinement (V-AMR) technique for the solution of the tip vortex flow and hence TVC observation in the propeller slipstream (Sezen and Atlar, 2021). In the authors' method, the grid is refined as local as possible in the tip vortex trajectory to reduce the computational cost of the solution using the V-AMR technique. This technique consists of two stages, namely 1st stage V-AMR and 2nd stage V-AMR. This two-stages V-AMR procedure enables a decrease in the solution's computational cost. In the 1st stage, the coarse grid reveals the tip vortex trajectory in the propeller slipstream. Following this, 2nd stage V-AMR is implemented using the fine grid resolution to observe the TVC. The authors have shown the feasibility and accuracy of this technique with different benchmark propellers using different numerical methods (e.g., RANS, DES and LES). Therefore, in this study, the same V-AMR technique was implemented to observe TVC for both model and full-scale propellers under uniform, inclined and non-uniform flow conditions. The cell size inside the vortex was kept at 0.2 mm for model scale applications, whereas it was kept at 0.68 mm for full-scale applications. This is because the tip vortex diameter in full-scale is larger than model scale propeller, and hence the cell size does not necessarily have to be the same order as in the model scale propeller. Nevertheless, it should be in a similar order relative to the propeller diameter. In this application, cell size in the model scale was enlarged with the scale ratio (i. e., $\lambda = 3.41$) and it was kept constant 0.68 mm for the observation of TVC in full-scale. The detailed information about the application of this technique can be found in the study of Sezen and Atlar (2021).

In addition to the cavitation modelling, the grid quality is also

important for the propeller URN prediction. The low-quality cells deteriorate the accuracy of the solution and create non-physical noise sources. The adapted grid should resolve/model the sound-generating turbulence scales and the cavitation dynamics and propagate the acoustic waves towards the locations of the receiver. The unstructured grid with hexahedral elements was used to discretise the computational domain. In order to increase the accuracy of the solution, the skewness of the cells was kept minimum. The smooth mesh transitions were achieved to decrease the non-physical numerical noise sources around the permeable noise surface. As the interfaces are the main source of non-physical noise, the grid quality was increased by identifying prism layers both inside and outside of the permeable noise surface. Also, the influence of grid resolution on propeller URN performance was investigated in our recent study, and hence detailed information about the effects of grid resolution on propeller URN can be found in Sezen et al. (2021).

The boundary layer was directly resolved for model scale applications, whereas the wall function was utilised for the boundary layer solution in full-scale applications. The total element count for model and full-scale propellers was calculated at approximately 24M and 32M, respectively. The numerical calculations were conducted with V-AMR (i.e., modelling sheet and tip vortex cavitation) and without the V-AMR technique (i.e., modelling only sheet cavitation) at all operating conditions to separate the contribution of TVC on overall URN. Other grid properties were kept constant between the solutions obtained with and without the V-AMR technique. The grid structure used in the numerical calculations with and without the V-AMR technique can be seen in Fig. 4.

3.2.3. Analysis properties

The numerical calculations used a segregated flow solver and SIMPLE algorithm for pressure-velocity coupling. The Hybrid Bounded Central Differencing Scheme (Hybrid-BCD) was utilised for the segregated solver to discretise convection terms in the momentum equations.

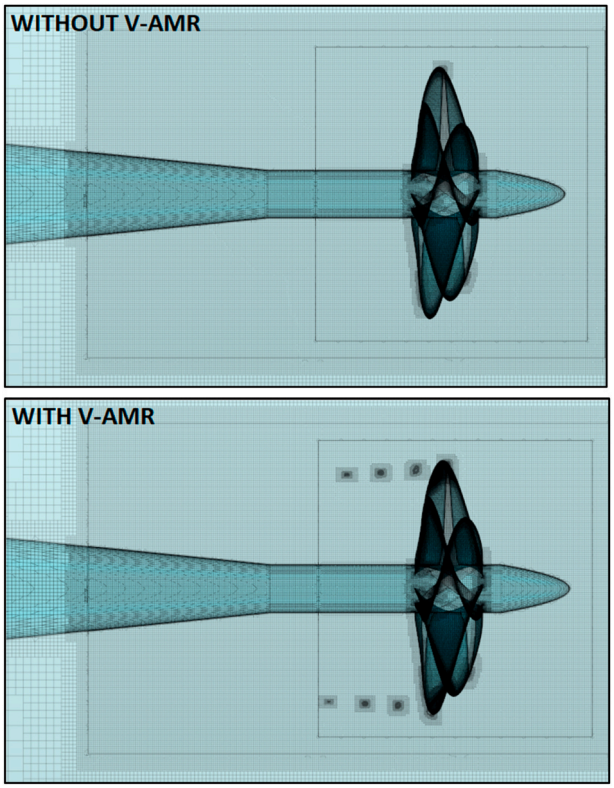

Fig. 4. Representation of grid resolution with and without V-AMR technique.

This scheme blends second-order upwind and bounded central differencing, and the blending factor is calculated according to the flow field features. This discretisation scheme is also advisable for DES methods. Furthermore, the second-order discretisation scheme was also utilised for the convection of turbulence terms and time (Star CCM+ 14.06, 2019). Timestep was selected at 0.5° of the propeller rotational rate at different operating conditions.

The multiphase VOF (Volume of Fluid) approach was coupled with the cavitation model for modelling the phases and hence the cavitation phenomena. For the convection term of the VOF approach, High-Resolution Interface Capturing (HRIC) was used to track the sharp interfaces between phases. The Eulerian mass transfer model, Schnerr-Sauer, was used to model the cavitation. In this model, the customisable cavitation parameters (i.e., nuclei density and diameter) can be changed as the water quality is important for the cavitation inception and its development (Korkut and Atlar, 2012). The nuclei density and diameter were set to 10^{12} ($1/m^3$) and 10^{-6} (m), respectively, based on our recent investigation of its effects on the sheet and tip vortex cavitation formation for model scale propeller (Sezen and Atlar, 2021). Also, for the full-scale propeller, the nuclei density and diameter were set to 10^{10} ($1/m^3$) and 10^{-6} (m), respectively.

The initialisation of the solution was carried out using a steady-state RANS approach. The same turbulence model (i.e., k-ω SST) was used during the initialisation process. This provided a consistent initial guess, ensuring that the problem was mathematically well-posed. In this process, Moving Reference Frame (MRF) was used for modelling the propeller rotational motion. Following the initialisation process, the DDES method was activated with the cavitation. The MRF approach was also switched to Rigid Body Motion (RBM) for the unsteady solution using DDES. During the first propeller rotation, the timestep was set to 1° of propeller rotational rate, and then it was reduced to 0.5° of propeller rotational rate. In this way, any possible stability issues related to cavitation phenomena were avoided. The acoustic pressures were collected during the six propeller revolutions when the flow field converged.

4. Results

4.1. Hydrodynamic results

The hydrodynamic performance coefficients obtained by CFD are compared with the available experimental and sea trial data at different operating conditions for model and full-scale propellers in Table 3. As shown in Table 3, the difference between CFD and experiment is found to be around 7% for thrust and torque coefficients under uniform and inclined flow conditions (i.e., C1 and C2) for model scale propeller. This is because different facilities performed the model experiments based on thrust identity and advance ratio identity during the RR test campaign. However, in the numerical calculations, the advance ratio identity (i.e., for C1 and C2) was used to eliminate the several iterative runs to find the same thrust coefficient as the experiment.

The torque identity was used for the non-uniform flow conditions (i.e., C5) in the model experiments. As the torque identity was not completely applied for CFD calculations at C5, the difference between

Table 3
Operating conditions for model and full-scale propellers.

Condition	EXPERIMENT & SEA-TRIAL		CFD	
	K_T	$10K_Q$	K_T	$10K_Q$
C1	0.244	0.341	0.262	0.365
C2	0.245	0.341	0.262	0.368
C3	–	–	0.257	0.356
C4	–	–	0.203	0.289
C5	–	0.318	0.237	0.346
C6	–	0.318	0.234	0.352

CFD and the experiment was found to be around 8% in terms of torque coefficient. The discrepancy between CFD and sea trial data is also found at 10% for torque coefficient at C6. This discrepancy also be related to scale effects in the wake distribution as it was measured in the towing tank. As the experimental and sea-trial data is not available for the full-scale propeller operating under uniform flow conditions (i.e., C3 and C4), only CFD results are given in Table 3.

The vortex structures in the propeller slipstream are compared with and without the V-AMR technique at C1 in Fig. 5. The iso-surface of the Q criterion was used to visualise the vortex structures. Also, the threshold value of the Q criterion is set to 5000 $1/s^2$ in Fig. 5. As shown in Fig. 5, the V-AMR technique is applied inside the rotating region, and the area is shown in green. With the application of the V-AMR technique, the pressure inside the vortex reduces compared to the base mesh (i.e., without the V-AMR technique). It is expected that the reduced pressure inside the vortex will enable observation of the TVC in the propeller slipstream. Additionally, the thinner vortex diameter is observed with the V-AMR technique as the actual TVC diameter is smaller than the tip vortex diameter. With the application of the V-AMR technique, two vortex structures emanating from the propeller's blade tip occur compared to the base mesh. Also, similar and persistent vortex structures can be seen with and without the V-AMR technique.

4.2. Cavitation extensions

The predicted cavitation extensions in the CFD were compared with the experiments conducted in the University of Genoa Cavitation tunnel and sea trial observations at different operating conditions. The numerical comparisons were performed in the presence of only sheet cavitation (i.e., without V-AMR technique) and sheet and TVC (i.e., with V-AMR technique) using iso-surface of volume fraction 0.1 ($\alpha_V = 0.1$).

Figs. 6 and 7 compare the cavitation observations between CFD and experiment for the model-scale propeller operating under uniform and inclined flow conditions (i.e., C1 and C2). Figs. 6 and 7 show that slightly more extended sheet cavitation towards the inner radii is observed in the CFD predictions compared to the experiment. As shown in Figs. 6 and 7, the stable TVC is successfully observed in the propeller slipstream with the V-AMR technique in both conditions. Similar

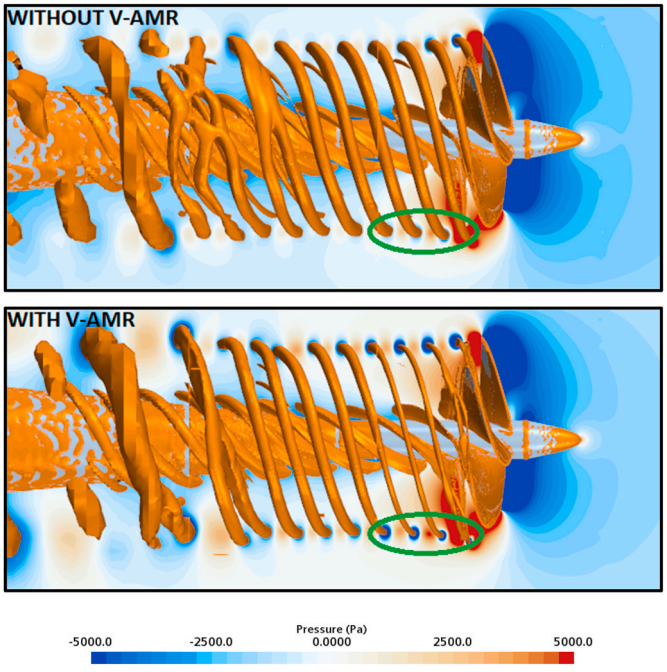

Fig. 5. The comparison of vortex structures with and without the V-AMR technique at C1. ($Q = 5000\ 1/s^2$).

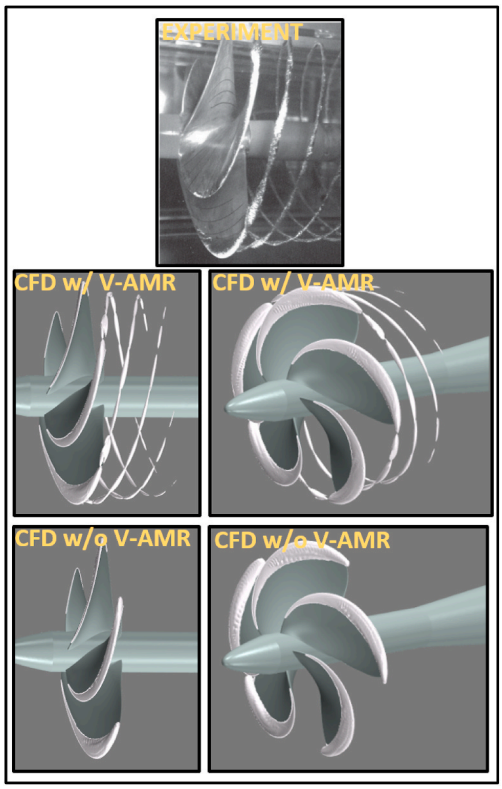

Fig. 6. The comparison of cavitation observations between the experiment and CFD together with and without the V-AMR technique at C1 ($\alpha_V = 0.1$).

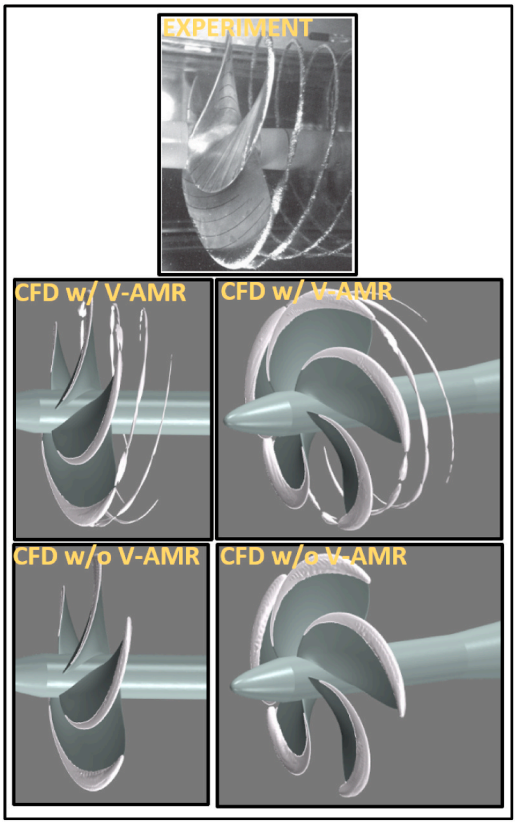

Fig. 7. The comparison of cavitation observations between the experiment and CFD together with and without the V-AMR technique at C2 ($\alpha_V = 0.1$).

cavitation extensions are observed at C1 and C2. Thus, the effects of shaft inclination on cavitation extension are not considerable. However, the cavitation dynamics can be stronger for the inclined flow condition (i.e., C2) than for the uniform flow condition (i.e., C1).

Fig. 8 shows the cavitation extensions for the full-scale propeller operating under uniform flow conditions (i.e., C3 and C4). As shown in Fig. 8, the higher blade loading manifests itself as a larger suction side sheet cavitation at C3 than C4. Similar to the model scale propeller's cavitation observations, applying the V-AMR technique enables better modelling of TVC in the propeller slipstream. The stable and structured TVC is observed at $J = 0.5$ (i.e., C4). However, the TVC is rather unstable and unstructured at $J = 0.4$ (i.e., C3) due to the increased blade loading. It is expected that this will consequently influence the cavitation dynamics and associated URN.

Figs. 9 and 10 show the cavitation extensions between CFD, experiment, and sea trial data at C5 and C6. According to sea trial observation, as shown in Fig. 10, the suction side sheet cavitation is large and covers around 25–30% of the propeller blades. Also, the cloudy and foamy sheet and TVC are present during the sea-trial observations. The cavitation observation is compared between the CFD and experiment at C5 in Fig. 9. The CFD calculations overpredict the sheet cavitation compared to the experiment as the sheet cavitation is present towards the inner radii in the CFD. This might be due to the slight differences in the wake distribution, as shown in Fig. 2. Similar TVC patterns are captured using CFD with less extensions in the propeller slipstream. However, the unstable and cloudy appearance of TVC could not be predicted in the model scale experiment and CFD calculations compared to the sea trial observations.

Fig. 10 also compares CFD predictions with the sea-trial observations in full scale. Akin to the model scale predictions, the unstable cavitation dynamics could not be predicted in the CFD. In addition to this, the sheet cavitation is slightly underpredicted in the CFD compared to sea-trial observation. V-AMR technique provides observation of TVC with much less intense vortex dynamics than the sea-trial observation.

4.3. URN predictions

4.3.1. Verification of the URN predictions

The verification studies are generally conducted for the propeller hydrodynamic performance predictions, and then suitable grid resolution is selected. In this process, the total element counts are kept as minimum as possible since the global performance characteristics can be predicted using coarse grid resolutions (i.e. less element counts) with good accuracy. However, as shown in our recent study (Sezen et al., 2021), the hydroacoustic solution is more dependent on grid resolution than the hydrodynamic solution. The insufficient grid resolution, which might be enough for global performance characteristics, leads to non-physical numerical noise issues, resulting in contamination of acoustic pressures. For this reason, the verification study in the hydroacoustic part of the solution should be carried out on its own by comparing the hydrodynamic and hydroacoustic pressures in the near field.

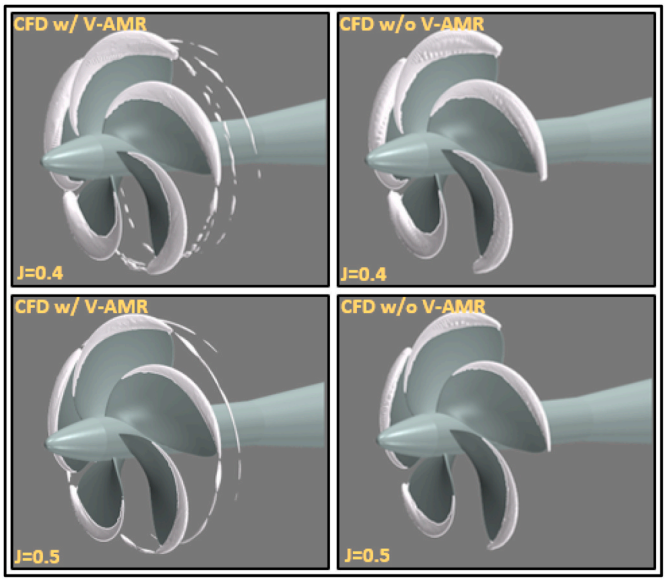

Fig. 8. The comparison of cavitation observations between with and without the V-AMR technique at C3 and C4 ($\alpha_V = 0.1$).

Strictly speaking, the incompressible flow assumption makes the sound speed infinite and denies acoustic propagation. Yet, the sound speed underwater is around 1500 m/s, and the marine propeller rotational rate and hence associated Mach number is very low compared to the propagation speed of sound. Also, the acoustic pressure predicted at a specific location is not the resulting value, which combines all possible sources travelling in the fluid. But, it is a rather instantaneous value, and contributions of all noise sources overlap together. The timeshift between the noise sources (compressibility or acoustic delay) affects the formation of acoustic pressure through the waveform and amplitude. This depends on relative motion between the receiver, source, and propagation speed. However, for marine propellers, the acoustic delays become negligible due to the low rotational speed and Mach number, as shown in the studies of Ianniello et al. (2013); Testa et al. (2021). Eventually, despite the inconsistency of incompressibility assumption, the comparison of hydrodynamic and hydroacoustic is still meaningful in near/mid-field and enables verification of the results. Moreover, the accuracy of both solvers (i.e., hydrodynamic and hydroacoustic parts) can also be proven with this comparison.

Within this framework, as an example, Fig. 11 shows the comparison of both pressures in the near field (i.e., z = 0.17m at the propeller plane from the centre of the blades) at C1. As shown in Fig. 11, both pressures are in agreement with each other, and the acoustic signal is purely characterised by BPF (Blade Passage Frequency). It should be noted that this agreement is valid everywhere in the near fields around the permeable surface for different operating conditions.

4.3.2. URN predictions with and without TVC in the time domain in the near field

In this section, the acoustic pressures obtained by only sheet cavitation and sheet and tip vortex cavitation were compared to show the influence of TVC on overall acoustic pressure levels in the near field. The pressures were recorded at the propeller plane, and the locations of the receivers were set to z = 0.171m and z = 0.5814m from the propeller blades' centre for model and full-scale propellers, respectively.

Fig. 12 shows the change in acoustic pressure levels in terms of amplitude and waveform at C1, C3, C4, C5, and C6. As shown in Fig. 12, the overall cavitating acoustic pressure signals are rather similar in a condition where only sheet cavitation is present and where the sheet and tip vortex cavitation is present at C1 for model scale and at C4 for the full-scale propeller. This is because the stable tip vortex dynamics are observed in the cavitation observations at C1 and C4 (see Figs. 6 and 8). Contrary to C1 and C4, the cavitating pressure signal changes with the contribution of TVC at C3, C5, and C6, where the unstable and more intense TVC are present. As shown in Fig. 12, the overall acoustic pressure signal shows higher amplitudes with the larger spikes (or irregularities) at C3, C5, and C6 (i.e., uniform and non-uniform flow conditions). These spikes can be associated with the possible bursting phenomena or large and violent cavitation dynamics, even though they could not be modelled as same as in the experiment and full-scale measurements using the CFD method. This results in an increase in noise levels over a broad frequency range. In addition to the TVC dynamics, the interaction of sheet and TVC can also be important for the increased noise level in the presence of TVC. Although the uniform flow condition is imposed for C3 and C4, the intense cavity dynamics

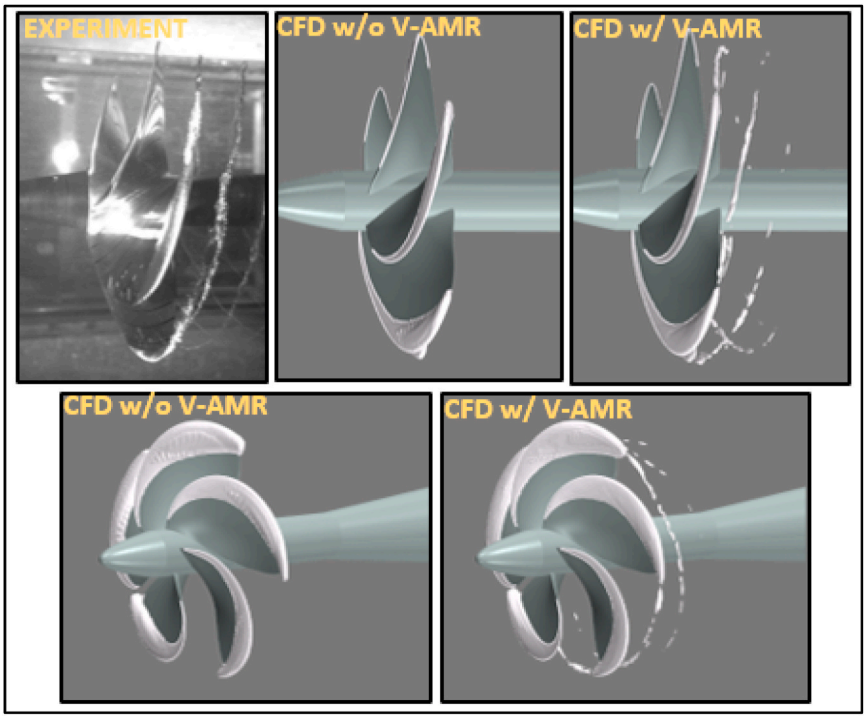

Fig. 9. The comparison of cavitation observations between the experiment and CFD together with and without the V-AMR technique at C5 ($\alpha_V = 0.1$).

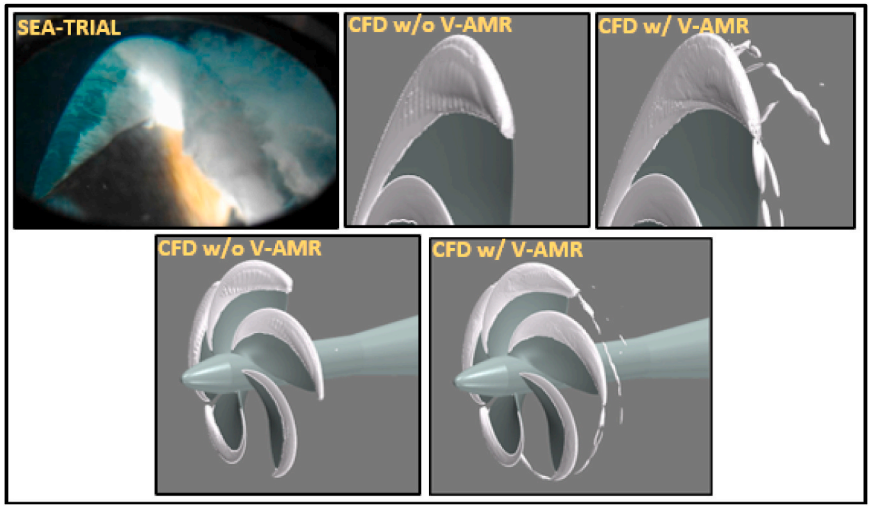

Fig. 10. The comparison of cavitation observations between the experiment and CFD together with and without the V-AMR technique at C6 ($\alpha_V = 0.1$).

observed at C3 cause irregularities with the TVC compared to C4.

In the study of Aktas et al. (2018), the investigation of cavitating pressure signals with different propellers was also performed experimentally to gain further insight into the noise driving mechanisms by applying the suitable signal processing methods. The authors adopted synchronised pressure pulse and noise measurements with the cavitation observations and explored the change in time-based pressure signal according to cavitation dynamics. Akin to the present study, the unstable and intense TVC created spikes in the acoustic signal at different operating conditions, and this was also considered due to the major cavitation events and cavitation collapse. Thus, the experimental study further supports the numerical findings of the present study on the influence of TVC in the time domain.

4.3.3. URN predictions with and without TVC in the frequency domain

The noise measurements and predictions are always presented with the noise spectrum in the frequency band. During the RR test campaign, the measurements were conducted by different facilities, and obtained results were compared with each other under uniform and inclined flow conditions (Tani et al., 2019b). Among the different facilities, in the present study, the numerical predictions for the model scale propeller were compared with the measurements performed in the University of Genoa Cavitation Tunnel due to the data availability for uniform, inclined, and non-uniform flow conditions. In the noise measurements, three receivers, namely H1, H2, and H3, were located inside and outside (i.e., in an acoustic chamber) the cavitation tunnel, as shown in Fig. 13. Hence, akin to the experimental set-up and receiver locations, the same receivers were positioned in the numerical calculations to replicate the experiment. The receiver H3 was utilised for C1 and C2, whereas the

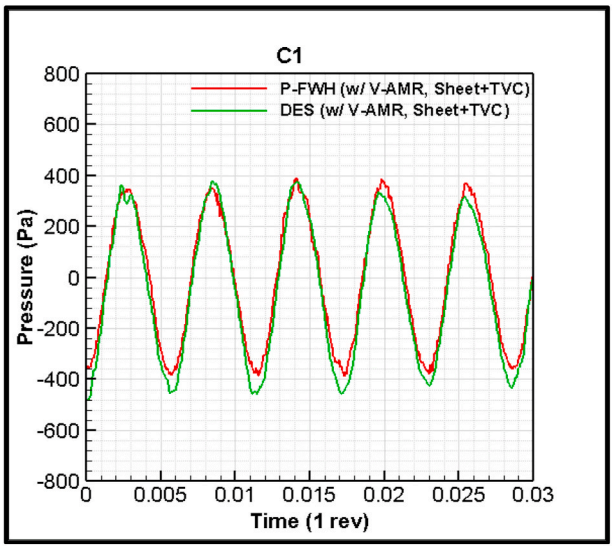

Fig. 11. The comparison of hydrodynamic and hydroacoustic pressures in the near field (z = 0.171m at the propeller plane from the propeller blades' centre).

receiver H1 was used at C5. In order to extrapolate the results from H3 to 1m and H1 to 1m, the spherical spreading loss was used in the numerical calculations due to the lack of data for the transfer functions used in the measurements.

Also, in the scope of the SONIC project (SONIC, 2012), the noise measurements were conducted with the Princess Royal vessel at different operating conditions, and a comprehensive database was obtained. The full-scale measurements were carried out with three receivers deployed at different depths. Later on, the results were corrected at 1m using the extrapolation procedure. Thus, the full-scale propeller URN predictions were compared with the full-scale measurements. In addition to the receivers positioned according to the model experiments, two more receivers were utilised, located at the propeller plane at 1m and 5.5m from the propeller blades' centre, to show the influence of TVC on overall cavitating propeller URN.

The noise spectrums are presented as power spectra (Pa^2) for model scale propeller (i.e., at C1 and C2) as in the experimental data, whereas the noise spectrums for the full-scale propeller at different operating conditions are presented as power spectral density (Pa^2/Hz) (i.e., C3, C4, C5 and C6). Also, the URN levels are presented in a 1/3 octave band.

It is to be noted that the details of the noise measurements and analysis procedures can be found for cavitation tunnel tests and full-scale measurements in the studies of Tani et al. (2017) and Brooker and Humphrey (2016), respectively.

Fig. 14 compares the URN predictions with the measured data in the model scale at C1, C2, and C5. As shown in Fig. 14, in the noise measurements, there is a high amplitude peak of around at 740Hz at C1, C2, and C5. As stated by Tani et al. (2017), this noise component is most likely because of the vibration of one of the foils supporting the receiver inside the tunnel. Also, this noise component could not be eliminated during the background noise measurements. Thus, it is not related to cavitating propeller URN.

Fig. 14 compares predicted URN results with the measured data at C1, C2, and C5. As shown in Fig. 14, the noise results are underpredicted in the low-frequency region of the noise spectrum at C1 and C2. Yet, the agreement between the CFD and measured data is good after 1 kHz. The underprediction of URN levels can be associated with the dissimilar cavitation dynamics predicted in the CFD calculations compared to the experiment at C1 and C2. Also, the mechanical noises in the tunnel can also be the reason for the discrepancy at certain frequencies. At C5, the numerical calculations overpredict the URN levels after 1 kHz. This can be related to the larger extension of sheet cavitation predicted in the CFD calculations compared to the experiment. At the medium-frequency range, the spectral hump, which is present in the measurement, dominates the noise spectrum. In contrast, the amplitude of the spectral hump is low in the numerical calculations at C5. This results in an underprediction of URN levels in the CFD calculations compared to the measured data in the low-frequency region of the noise spectrum.

The influence of TVC on overall URN levels can also be seen in Fig. 14 at C1, C2, and C5. In general, the sheet and tip vortex cavitation are stable under uniform flow conditions and do not generate large cavitating volume variations. Hence, the sheet cavitation produces higher noise levels at the broadband part of the noise spectrum, and this can be accounted for by the breakup and collapse of small cavities shed by the sheet at the trailing edge of the propeller blades. In this situation, the stable tip vortex can produce a high and narrowband peak at the low-medium frequency region because of the vortex cavity pulsation. However, the spectral peak characteristics depend on the operating conditions and vortex dynamics. When the large and persistent vortices are present in the propeller slipstream, the vortex pulsation can be considered the main noise mechanism. Also, when the other mechanisms such as cavitation volume variations because of the wake flow, cavity collapses, and bursting phenomena are dominant, the severity of the peak can be less, and the created acoustic energy with the other noise mechanisms is distributed over the noise spectrum. Eventually, the noise spectrum characterised by the only TVC or together with the sheet cavitation can be found in different forms depending on the dynamic of vortices and cavitation (Tani et al., 2019a). As shown in Fig. 14, akin to the near field cavitating propeller signal, the contribution of TVC to the overall propeller URN is not considerable at C1, where the uniform flow and stable TVC are present. At C2, the shaft inclination creates cavitation volume variations, and it manifests itself in higher URN levels in the numerical calculation, which is performed in the presence of sheet and tip vortex cavitation. When the non-uniform wakefield is concerned (i.e., C5), which is the main noise-producing mechanism because of the change in cavitation volume of sheet and vortex cavitation, the influence of TVC on overall URN levels can be clearly seen over the noise spectrum in Fig. 14. The URN levels increase up to 15 dB by the contribution of TVC compared to the URN predictions in the presence of only sheet cavitation. Moreover, the spectral hump, which is characterised by the vortex dynamics as explained above, can be seen in URN predictions obtained by CFD between 600Hz and 1 kHz at C5, whereas it is not distinct at C1 and C2 as same as at C5.

In the past, cavitation tunnel experiments were conducted by Pennings et al. (2015) to explore the relation of tip vortex cavity dynamics with the cavitating propeller URN using the two-bladed model propeller. The results showed that the tip vortex cavity observed under uniform flow conditions did not generate noise with considerable amplitude above the tunnel background. However, a significant broadband contribution was observed due to the cavity dynamics when the tests were carried out under non-uniform flow conditions. Thus, the experimental study also supports the present study's findings in terms of TVC influence on propeller URN under uniform and non-uniform flow conditions for the model scale propeller.

The full-scale propeller URN predictions are compared with each other at C3 and C4 to explore the influence of TVC on overall propeller URN at C3 and C4 in Fig. 15. As shown in Fig. 15, with an increase in blade loading, associated cavitation extensions, and its dynamics, the URN levels increase from C4 to C3. Similar to the model scale propeller operating under uniform flow conditions (i.e., C1), at C4, stable TVC dynamics do not produce considerable sound compared to the URN predictions in the presence of only sheet cavitation. However, unlike the model scale propeller URN predictions under uniform flow conditions (i.e., C1) and C4, the TVC increases the URN levels considerably at C3 (i.e., under uniform flow conditions). This is because the rather unstable and irregular TVC dynamics are present at C3 compared to the cavitation dynamics observed at C4. Although the larger cavitation volume variations are not expected under uniform flow conditions, the breakup of

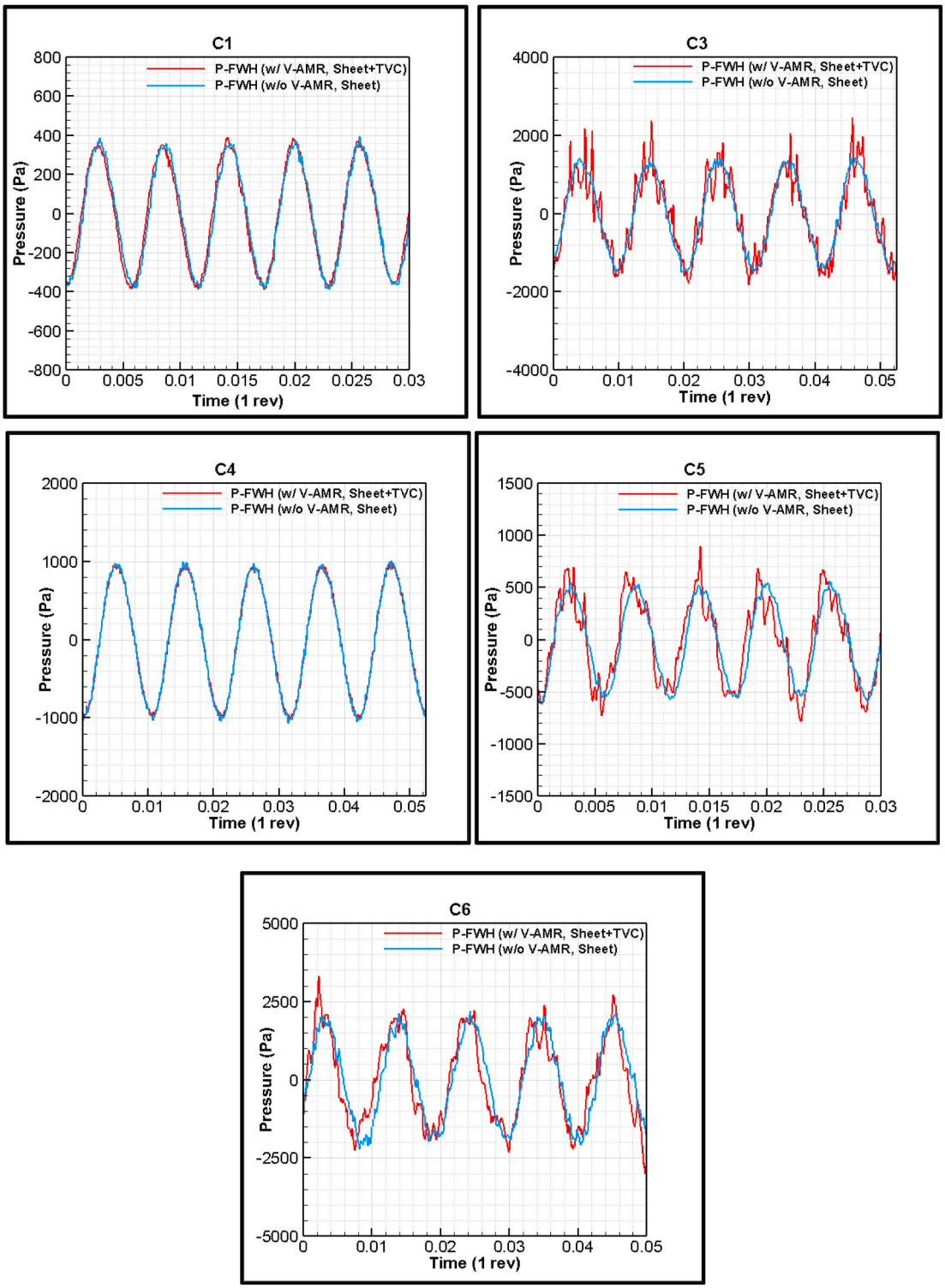

Fig. 12. The comparison of cavitating acoustic signals in the time domain with and without TVC in the near field.

the cavity vortices together with the sheet cavitation interaction seems to be one of the reasons for the considerable URN increase with the TVC at C3. This breakup of vortices can further contribute to the nonlinear noise sources. Also, the intense cavity dynamics manifest itself as a spectral hump around 600Hz and 1 kHz at C3 in full-scale.

Fig. 16 shows the comparison of URN predictions with the full-scale measurements at C6. As shown in Fig. 16, the results are in good agreement with each other up to 1 kHz. After 1 kHz, the numerical calculations underpredict the URN levels compared to full-scale measurements. This can be associated with the lack of nonlinear noise sources represented by turbulence, vorticity, and TVC dynamics predicted in the CFD calculations. Similar to model scale URN predictions in the presence of TVC (i.e., C5), the non-uniform flow increases the URN levels by introducing the TVC in the numerical calculations. The characteristics hump is also somewhat present in the mid-frequency range in the numerical predictions in the presence of TVC, as in the full-scale measurements.

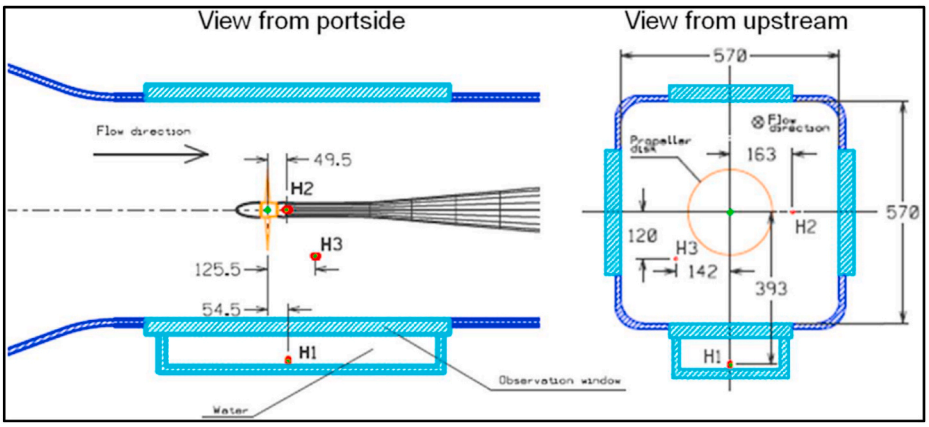

Fig. 13. The receiver locations for the URN measurements during the experiments in UNIGE (Tani et al., 2017).

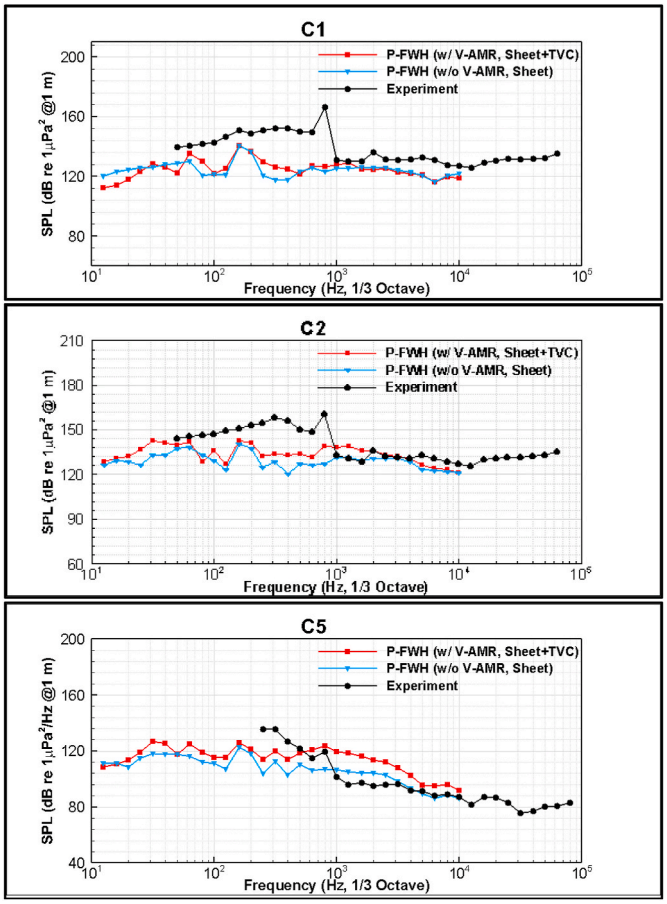

Fig. 14. The comparison of URN levels between CFD and measured data at 1m and CFD predictions with and without the TVC at C1, C2 and C5.

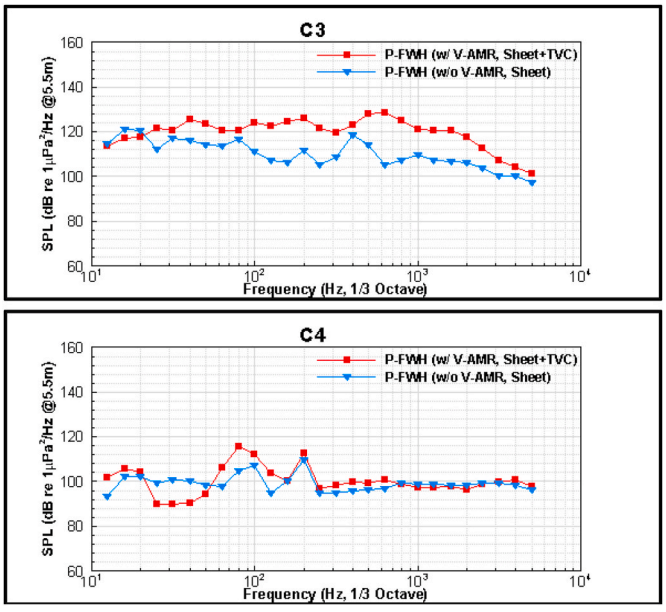

Fig. 15. The comparison of URN levels between the CFD predictions carried out with and without the TVC at C3 and C4.

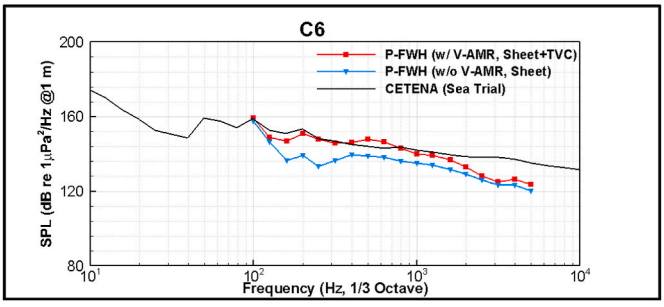

Fig. 16. The comparison of URN levels between CFD and full-scale measurements at 1m and with and without the TVC at C6.

5. Conclusion

The present study presented a more in-depth investigation into the effect of TVC on propeller URN for the model and full-scale propellers, shedding further light on the contribution of the TVC to the propeller hydrodynamic and hydroacoustic performance by using the DES and permeable FWH acoustic analogy. In the numerical calculations, the model and full-scale benchmark propeller of the Newcastle University research vessel, The Princess Royal, was operating under uniform, inclined and non-uniform flow conditions. The CFD verification study was conducted for the hydroacoustic part of the solution. The propeller performance characteristics, cavitation extensions, and propeller URN predictions were comprehensively validated with the experimental and sea trial data with The Princess Royal model and full-scale vessel, respectively. The main finding of the study can be summarised as follows.

- The application of the V-AMR technique changed the flow properties inside the vortex. Although similar vortex extensions were observed in the propeller slipstream between the base mesh and the refined mesh, the TVC could only be observed in the propeller slipstream at all operating conditions both in model and full-scale using the V-AMR technique.
- Similar sheet cavitation extensions were observed between the CFD and experiment. However, the sheet cavitation was slightly more extended towards inner radii in the CFD compared to the experimental data under the uniform and inclined flow conditions (i.e., C1 and C2).
- Under the non-uniform flow conditions in the model scale (i.e., C5), the sheet cavitation extension predicted in the CFD agreed with the sea trial data. However, its extension was overpredicted compared to the model scale observations. The sheet cavitation was slightly underpredicted in the CFD compared to sea trial data in full scale (i.e., C6).
- The time-based acoustic pressures showed that the stable TVC dynamics, as observed at C1 and C4, did not change the waveform and amplitude of the signal compared to the configuration where only the sheet cavitation was modelled. However, when the propeller was operating in the inclined shaft and under non-uniform flow conditions, the TVC created larger spikes in the acoustic pressures. These spikes can be associated with strong cavity dynamics and other cavitation events, mainly with the possible collapsing/bursting phenomena compared to the configuration where the only sheet cavitation was modelled.
- The comparison of the propeller URN predictions showed that the noise results were underpredicted by the CFD compared to the experimental measurements under the uniform and inclined flow conditions, particularly up to 1 kHz. However, due to the more extensive sheet cavitation observed in the CFD compared to the experiment, the propeller URN levels were overpredicted compared to measured data under non-uniform flow conditions (i.e., C5) in the model scale. The full-scale URN comparison showed a good agreement between the CFD and full-scale measurements up to 1 kHz.
- The comparisons obtained for the configurations with and without the TVC in the noise spectrums showed that the stable TVC did not create significant vortex pulsation. Hence, the propeller URN levels did not lead to a considerable change in the contribution of TVC in the numerical calculations. Yet, the propeller URN levels increased considerably when the cavitation volume variations and pulsation were stipulated with the unstable TVC, as in C2, C3, C5 and C6. Furthermore, the maximum increase with the contribution of TVC was observed at C5 and C6, where the non-uniform wake field was present.
- The unstable TVC and its cavitation dynamics manifested themselves as a spectral hump in the noise spectrum at the medium frequency range, particularly at C3, C5 and C6.
- This study showed the capabilities of the V-AMR technique for including the effects of TVC on overall propeller URN. Thus, the proposed methodology, including URN modelling, can be used for the investigation of URN for newly designed, existing and retrofit marine propellers.
- This study can be further improved using the more advanced hydrodynamic method (i.e., LES) cavitation model. Also, the compressibility assumption can be also adopted for the propeller URN predictions.

CRediT authorship contribution statement

Savas Sezen: Conceptualization, Methodology, Software, Validation, Investigation, Data curation, Writing – original draft, Writing – review & editing, Visualization. **Mehmet Atlar:** Investigation, Resources, Writing – review & editing, Supervision, Project administration.

Declaration of competing interest

The authors declare that they have no known competing financial interests or personal relationships that could have appeared to influence the work reported in this paper.

Data availability

No data was used for the research described in the article.

Acknowledgements

The first author was sponsored by Stone Marine Propulsion Ltd of the UK and the University of Strathclyde during his PhD study. Results were obtained using the ARCHIE-WeSt High-Performance Computer (www.archie-west.ac.uk) based at the University of Strathclyde. The authors also thank Dr Giorgio Tani for providing the experimental data.

References

Aktas, B., Atlar, M., Fitzsimmons, P., Shi, W., 2018. An advanced joint time-frequency analysis procedure to study cavitation-induced noise by using standard series propeller data. Ocean Eng. 170, 329–350. https://doi.org/10.1016/j.oceaneng.2018.10.026.

Asnaghi, A., Svennberg, U., Bensow, R.E., 2020a. Large Eddy Simulations of cavitating tip vortex flows. Ocean Eng. 195 https://doi.org/10.1016/j.oceaneng.2019.106703.

Asnaghi, A., Svennberg, U., Gustafsson, R., Bensow, R.E., 2020b. Propeller tip vortex mitigation by roughness application. Appl. Ocean Res. 102449 https://doi.org/10.1016/j.apor.2020.102449.

Astolfi, J.A., Billard, J.Y., Dorange, P., Fruman, D.H., 1998. Pressure fluctuations associated with tip vortex and surface cavitation. In: Proceedings of the ASME Fluids Engineering Division Summer Meeting. Washington, DC, USA.

Atlar, M., Aktas, B., Samspon, R., Fitzsimmons, P., Fetherstonhaug, C., 2013. A multi-purpose marine science and technology research vessel for full-scale observations and measurements. In: 3rd International Conference on Advanced Model Measurement Technologies for the Marine Industry, AMT'13. Gdansk, Poland.

Barker, S.J., 1976. Measurements of hydrodynamic noise from submerged hydrofoils. J. Acoust. Soc. Am. 59, 1095. https://doi.org/10.1121/1.380963.

Bensow, R.E., Liefvendahl, M., 2016. An acoustic analogy and scale-resolving flow simulation methodology for the prediction of propeller radiated noise. In: 31st Symposium on Naval Hydrodynamics Monterey, California. Monterey, California, USA, pp. 1–19.

Berger, Stephan, 2018. Numerical analysis of propeller-induced higher-order pressure fluctuations on the ship hull. In: Institute for Fluid Dynamics and Ship Theory (FDS), Hamburg University of Technology (TUHH). PhD thesis.

Bosschers, J., 2018. Propeller Tip-Vortex Cavitation and its Broadband Noise, PhD Thesis. Universtiy of Twente, Netherlands.

Brooker, A., Humphrey, V., 2016. Measurement of radiated underwater noise from a small research vessel in shallow water. Ocean Eng. 120, 182–189. https://doi.org/10.1016/j.oceaneng.2015.09.048.

Di Francescantonio, P., 1997. A new boundary integral formulation for the prediction of sound radiation. J. Sound Vib. 202, 491–509. https://doi.org/10.1006/jsvi.1996.0843.

Farassat, F., 2007. Derivation of formulations 1 and 1A of Farassat. In: NASA/TM-2007-214853, pp. 1–25.

Feder, Dag-Frederik, 2021. Evolution of trailing vortices around a ship hull at large drift angle. In: Institute for Fluid Dynamics and Ship Theory (FDS),Hamburg University of Technology (TUHH). PhD thesis.

Ffowcs Williams, J.H., Hawkings, D.L., 1969. Sound generation by turbulence and surfaces in arbitrary motion. Philos. Trans. R. Soc. Lond. Ser. A, Math. Phys. Sci. 264, 321–342. https://doi.org/10.1098/rsta.1969.0031.

Fujiyama, K., Nakashima, Y., 2017. Numerical prediction of acoustic noise level induced by cavitation on ship propeller at behind-hull condition. In: Fifth International Symposium on Marine Propulsion, SMP'17. Espoo, Finland.

Higuchi, H., Arndt, R.E.A., Rogers, M.F., 1989. Characteristics of tip vortex cavitation noise. In: Journal of Fluids Engineering, Transactions of the ASME, pp. 495–501. https://doi.org/10.1115/1.3243674.

Ianniello, S., Muscari, R., Di Mascio, A., 2014a. Ship underwater noise assessment by the acoustic analogy, part III: measurements versus numerical predictions on a full-scale ship. J. Mar. Sci. Technol. 19, 125–142. https://doi.org/10.1007/s00773-013-0228-z.

Ianniello, S., Muscari, R., Di Mascio, A., 2014b. Ship underwater noise assessment by the Acoustic Analogy part II: hydroacoustic analysis of a ship scaled model. J. Mar. Sci. Technol. 19, 52–74. https://doi.org/10.1007/s00773-013-0236-z.

Ianniello, S., Muscari, R., Di Mascio, A., 2013. Ship underwater noise assessment by the acoustic analogy. Part I: nonlinear analysis of a marine propeller in a uniform flow. J. Mar. Sci. Technol. 18, 547–570. https://doi.org/10.1007/s00773-013-0227-0.

Kimmerl, J., Mertes, P., Abdel-Maksoud, M., 2021. Application of large eddy simulation to predict underwater noise of marine propulsors. Part 1: cavitation dynamics. J. Mar. Sci. Eng. 9, 792. https://doi.org/10.3390/JMSE9080792.

Konno, A., Wakabayashi, K., Yamaguchi, H., Maeda, M., Ishii, N., Soejima, S., Kimura, K., 2002. On the mechanism of the bursting phenomena of propeller tip vortex cavitation. J. Mar. Sci. Technol. 6, 181–192. https://doi.org/10.1007/s007730200006.

Korkut, E., Atlar, M., 2012. An experimental investigation of the effect of foul release coating application on performance, noise and cavitation characteristics of marine propellers. Ocean Eng. 41, 1–12. https://doi.org/10.1016/j.oceaneng.2011.12.012.

Korkut, E., Takinaci, A.C., 2013. 18M research vessel wake measurements. In: Faculty of Naval Architecture and Ocean Engineering, Istanbul Technical University. Istanbul, Turkey.

Krasilnikov, V., 2019. CFD modelling of hydroacoustic performance of marine propellers: predicting propeller cavitation. In: Numerical Towing Tank Symposium, NuTTS'2019. Tomar, Portugal.

Lafeber, F.H., Bosschers, J., Van Wijngaarden, E., 2015. Computational and experimental prediction of propeller cavitation noise. MTS/IEEE Ocean. https://doi.org/10.1109/OCEANS-GENOVA.2015.7271654, 2015 - Genova Discov. Sustain. Ocean Energy a New World.

Li, D.Q., Hallander, J., Johansson, T., 2018. Predicting underwater radiated noise of a full scale ship with model testing and numerical methods. Ocean Eng. 161, 121–135. https://doi.org/10.1016/j.oceaneng.2018.03.027.

Lidtke, A.K., Humphrey, V.F., Turnock, S.R., 2016. Feasibility study into a computational approach for marine propeller noise and cavitation modelling. Ocean Eng. 120, 152–159. https://doi.org/10.1016/j.oceaneng.2015.11.019.

Lidtke, A.K., Vaz, G., Lloyd, T., 2019. Acoustic modelling of a propeller subject to non-uniform inflow. In: Proceedings of 6th International Symposium on Marine Propulsors, SMP2019, Rome, Italy.

Lloyd, T., Vaz, G., Rijpkema, D., Reverberi, A., 2017. Computational fluid dynamics prediction of marine propeller cavitation including solution verification. In: Fifth International Symposium on Marine Propulsors, SMP'17.

Maines, B., Arndt, R.E.A., 1997. The case of the singing vortex. J. Fluid Eng. 119, 271–276. https://doi.org/10.1115/1.2819130.

Muzaferija, S., Papoulias, D., Peric, M., 2017. VOF simulations of hydrodynamic cavitation using the asymptotic and classical Rayleigh-Plesset models. In: Fifth International Symposium on Marine Propulsion, Smp'17. Espoo, Finland.

Nitzkorski, Z., 2015. A Novel Porous Ffowcs-Williams and Hawkings Acoustic Methodology for Complex Geometries. Faculty of the Graduate School of the University of Minnesota. PhD thesis.

Pennings, P., Westerweel, J., van Terwisga, T., 2016. Cavitation tunnel analysis of radiated sound from the resonance of a propeller tip vortex cavity. Int. J. Multiphas. Flow 83, 1–11. https://doi.org/10.1016/j.ijmultiphaseflow.2016.03.004.

Pennings, P., Westerweel, J., Van Terwisga, T., 2015. Sound signature of propeller tip vortex cavitation. In: 9th International Symposium on Cavitation (CAV2015). Institute of Physics Publishing. https://doi.org/10.1088/1742-6596/656/1/012186.

Raestad, A.E., 1996. Tip vortex index-an engineering approach to propeller noise prediction. Nav. Archit. 10–11. ISSN 03060209.

Schnerr, G.H., Sauer, J., 2001. Physical and numerical modeling of unsteady cavitation dynamics. In: 4th International Conference on Multiphase Flow. New Orleans, USA.

Sezen, S., Atlar, M., 2021. An alternative Vorticity based Adaptive Mesh Refinement (V-AMR) technique for tip vortex cavitation modelling of propellers using CFD methods. Ship Technol. Res. 69, 1–21. https://doi.org/10.1080/09377255.2021.1927590.

Sezen, S., Bal, S., 2020. Computational and empirical investigation of propeller tip vortex cavitation noise. China Ocean Eng. 34, 232–244. https://doi.org/10.1007/s13344-020-0022-8.

Sezen, S., Cosgun, T., Yurtseven, A., Atlar, M., 2021. Numerical investigation of marine propeller Underwater Radiated Noise using acoustic analogy part 1: the influence of grid resolution. Ocean Eng. 220, 108448 https://doi.org/10.1016/j.oceaneng.2020.108448.

Sezen, S., Cosgun, T., Yurtseven, A., Atlar, M., 2020. Numerical investigation of marine propeller underwater radiated noise using acoustic analogy part 2: the influence of eddy viscosity turbulence models. Ocean Eng. 220, 108353 https://doi.org/10.1016/j.oceaneng.2020.108353.

SONIC, 2012. Suppression of Underwater Noise Induced by Cavitation. EC-FP7, Grant Agreement No: 2012, 314394.

Spalart, P.R., Jou, W.-H., Strelets, M., Allmaras, S.R., Research, U.S.A.F.O. of S., 1997. Comments on the feasibility of LES for wings, and on a hybrid RANS/LES approach. In: Proceedings of First AFOSR International Conference on DNS/LES. Greyden Press.

Star CCM+ 14.06, 2019. User Guide. Siemens.

Stark, C., Shi, W., 2021. Hydroacoustic and hydrodynamic investigation of bio-inspired leading-edge tubercles on marine-ducted thrusters. R. Soc. Open Sci. 8, 210402 https://doi.org/10.1098/RSOS.210402.

Strasberg, M., 1986. Hydrodynamic cavitation noise. In: International Symposium on Cavitation and Multiphase Flow Noise, ASME Winter Annual Meeting. Anaheim, California, USA.

Taehyung, K., Jonghoon, J., Sunghan, C., Sunghoon, K., Wonho, J., 2016. Numerical and experimental prediction methods of cavitation noise radiated by underwater propellers. In: Proceedings of the 22nd International Congress on Acoustics. Hyundai Heavy Industries, Buenos Aires, Argentina.

Tani, G., Aktas, B., Viviani, M., Atlar, M., 2017. Two medium size cavitation tunnel hydroacoustic benchmark experiment comparisons as part of a round robin test campaign. Ocean Eng. 138, 179–207. https://doi.org/10.1016/j.oceaneng.2017.04.010.

Tani, G., Aktas, B., Viviani, M., Yilmaz, N., Miglianti, F., Ferrando, M., Atlar, M., 2019a. Cavitation tunnel tests for "The Princess Royal" model propeller behind a 2-dimensional wake screen. Ocean Eng. 172, 829–843. https://doi.org/10.1016/j.oceaneng.2018.11.017.

Tani, G., Viviani, M., Felli, M., Lafeber, F.H., Lloyd, T., Aktas, B., Atlar, M., Turkmen, S., Seol, H., Hallander, J., Sakamoto, N., 2020. Noise measurements of a cavitating propeller in different facilities: results of the round robin test programme. Ocean Eng. 213, 107599 https://doi.org/10.1016/j.oceaneng.2020.107599.

Tani, G., Viviani, M., Felli, M., Lafeber, F.H., Lloyd, T., Atlar, M., Seol, H., Hallander, J., Sakamoto, N., Kamiirisa, H., 2019b. Round robin test on radiated noise of a cavitating propeller. In: Proceedings of 6th International Symposium on Marine Propulsors, SPM'19. Rome, Italy.

Testa, C., Porcacchia, F., Zaghi, S., Gennaretti, M., 2021. Study of a FWH-based permeable-surface formulation for propeller hydroacoustics. Ocean Eng. 240, 109828 https://doi.org/10.1016/J.OCEANENG.2021.109828.

Testa, C., Procacchia, F., Greco, L., Muscari, R., 2018. Effectiveness of boundary element method hydrodynamic data for propeller hydroacoustics. In: A. Yucel Odabasi Colloquium Series 3rd International Meeting-Progress in Propeller Cavitation and its Consequences. Istanbul, Turkey.

van Terwisga, T.J.C., 2006. Cavitation research on ship propellers. In: Sixth International Symposium on Cavitation, CAV2006. Wageningen, The Netherlands.

Wang, M., Freund, B., Lele, J.K., S., 2018. Computational prediction of flow-generated sound. Annu. Rev. Fluid Mech. 50, 77–103. https://doi.org/10.1146/annurev.fluid.

Van Wijngaarden, E., 2011. Prediction of Propeller-Induced Hull-Pressure Fluctuations. University of Twente, Netherlands. PhD Thesis.